Two dimensional IR-FID-CPMG acquisition and adaptation of a maximum entropy reconstruction

Corinne C. Rondeau-Mouro, R. Kovrlija, E. van Steenberge, Saïd Moussaoui

Two dimensional IR-FID-CPMG acquisition and adaptation of a maximum entropy reconstruction

C. Rondeau-Mouro [a,c,*], R. Kovrlija [a,c], E. Van Steenberge [a,c], S. Moussaoui [b]

[a] IRSTEA, UR OPAALE, 17 Avenue de Cucillé, CS 64427, F-35044 Rennes, France
[b] IRCCyN, CNRS UMR 6597, 1 rue de la Noë, BP 92101, F-44321 Nantes Cedex 03, France
[c] Université Européenne de Bretagne, France

By acquiring the FID signal in two-dimensional TD-NMR spectroscopy, it is possible to characterize mixtures or complex samples composed of solid and liquid phases. We have developed a new sequence for this purpose, called IR-FID-CPMG, making it possible to correlate spin–lattice T_1 and spin–spin T_2 relaxation times, including both liquid and solid phases in samples. We demonstrate here the potential of a new algorithm for the 2D inverse Laplace transformation of IR-FID-CPMG data based on an adapted reconstruction of the maximum entropy method, combining the standard decreasing exponential decay function with an additional term drawn from Abragam's FID function. The results show that the proposed IR-FID-CPMG sequence and its related inversion model allow accurate characterization and quantification of both solid and liquid phases in multiphasic and compartmentalized systems. Moreover, it permits to distinguish between solid phases having different T_1 relaxation times or to highlight cross-relaxation phenomena.

1. Introduction

More and more companies have in recent years proposed new compact Nuclear Magnetic Resonance (NMR) systems, which are very affordable, versatile, high performance and easy-to-use instruments. These low-resolution (or Time Domain) NMR spectrometers (TD-NMR) are particularly interesting for process control and formulation in food industries and are conventionally used to measure the solid fat content of fat blends used for butters, margarines and oils on the basis of well-known official methods from the American Oil Chemists' Society (AOCS) [1–3]. Low-field spectrometers can also be equipped with linear magnetic field gradient units, allowing diffusion measurements, which can be very useful for instance in characterizing emulsions. The analytical potential of these spectrometers is however much wider. Based on longitudinal (T_1) and transverse (T_2) relaxation time measurements [4–6], benchtop NMR equipment can also be used to obtain quantitative information about the composition and the liquid/solid state of multiphasic compounds in products other than food, such as semi-clathrate hydrates, cements, wood or rocks in oil and gas production [7,8]. NMR relaxation times are not only sensitive to the physical state of molecules (for example liquid or solid) [9], but are also sensitive to the liquid/solid interface in porous materials [10–15] and to chemical and diffusional exchanges of protons between molecules and compartments [16]. These phenomena result in distributions of relaxation times related to the distribution and mobility of molecules in samples subjected to various dipolar interactions. Analysis of solid samples is currently performed by the acquisition of Free Induction Decay (FID) or solid echo signals. Applications for these sequences were demonstrated in the early 1970s when several low-field NMR methods were introduced, allowing rapid and precise determination of the solid fat content (SFC) in fatty products (see references in [9]). Later, with the improvement of the electronic and computational specifications of TD-NMR spectrometers, coupled FID-CPMG data (Fig. 1a) could be acquired [17] and extended to other food products [18,19].

Extraction of the relaxation parameters from a decaying signal measured using CPMG, FID, or the classical inversion recovery (IR) sequence corresponds to a numerical inversion of the Laplace transform. Such signal processing task is known to be a large-scale inverse problem. One of the approaches to analyzing multi-exponential data consisted of a Non-Negative Least Squares (NNLS) fitting procedure [20], under suitable regularization constraints. This can be implemented, for instance, by the CONTIN software package [21]. Methods based on the inverse Laplace transform

* Corresponding author at: Irstea, UR OPAALE, CS 64426, 17 Avenue de Cucillé, 35044 Rennes Cedex, France. Fax: +33 (0)223482115.
E-mail address: corinne.rondeau@irstea.fr (C. Rondeau-Mouro).

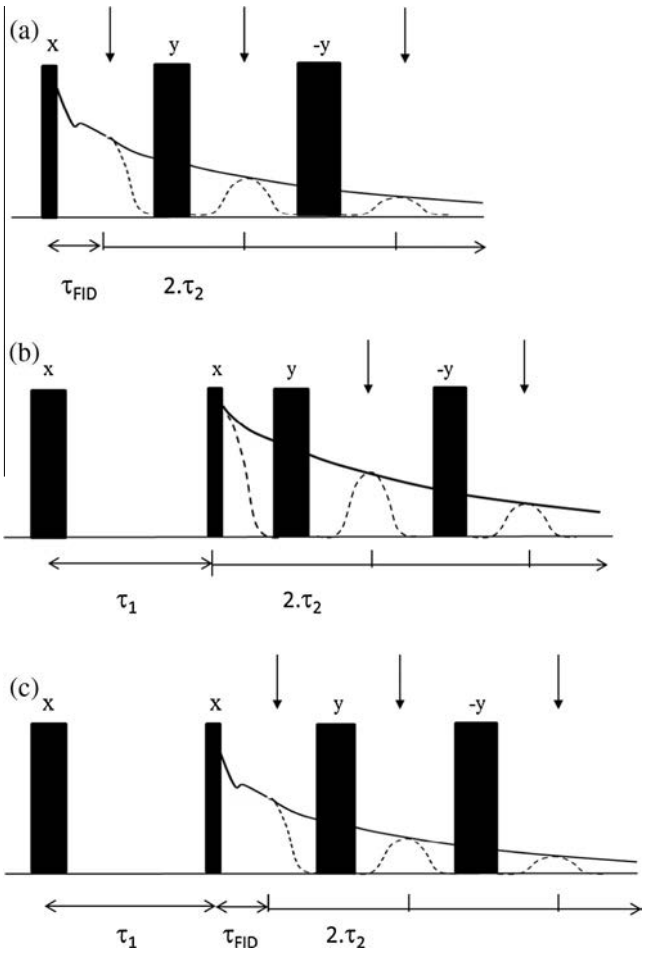

Fig. 1. Pulse sequence scheme for FID-CPMG (a), and T_1–T_2 measurements via inversion recovery followed by CPMG (b) or by FID-CPMG (c) acquisition. In each diagram, the thin and thick rectangles represent 90° and 180° RF pulses, respectively. The arrows indicate the time when the receiver gate is opened for acquisition. τ_1 is the first time evolution after inversion of magnetization, τ_{FID} the FID duration and ($2.\tau_2$), the echo time of CPMG.

were developed later, but these showed numerical instability in the sense that a small noise in the data can cause considerable changes in the resulting distribution (see references in [22–25]). However, the method used by Mariette et al., consisting of comparing Marquardt and Maximum Entropy Method (MEM) fitting of CPMG signals, was more successful [19]. Only a few publications have referred to the curve-fitting of combined FID-CPMG data [17]. Most publications have tended to use predefined functions generally based on NNLS algorithms and separate fitting of FID and CPMG signals because of the different mobility regimes of molecules described by Gaussian, Pake, and Lorentzian (exponential) functions [17,19,26]. For the same reason, no method based on MEM has been developed until now to adjust combined FID-CPMG data. In addition to this unidimensional approach, that is easily applied in the food and petroleum industries, two-dimensional (2D) cross-correlation relaxation is one of the major developments in low-field NMR in the last fifteen years. As in high-field NMR spectroscopy, the principle of the signal acquisition is based on the evolution of spin systems while applying two or more independent variables, such as time, instead of chemical shift or other specific magnetic interaction. In relaxometry, spins can be differentiated or correlated due to their different T_1 and T_2 relaxation times, characteristic of molecular species and specific dynamics depending on the molecule environment and dipolar interactions. Research has already benefited from this two-dimensional technique for many applications, from cement-based materials and rock to food and biological products, such as plants and wood (see references in [27]). However, these studies would not have been possible without the technical advances in computer hardware and the development of fast and efficient algorithms for two-dimensional inverse Laplace transformations. The first reconstruction of two dimensional relaxation distributions was successfully performed using NNLS and imposing positivity constraints on the solution amplitudes [28]. As a commonly used regularization method, the maximum entropy method (MEM) has shown satisfactory results for the reconstruction of 2D T_1–T_2 distributions [29–32]. However, none of these reports have involved measurement of the solid phase in samples. NMR experiments to date have mostly been based on T_1-weighted CPMG acquisitions (Fig. 1b), although several two-dimensional hybrid pulse sequences based on the multi-window analysis of T_1-weighted FID signals have been developed [33,34]. There are two main reasons to explain the lack of simultaneous studies of solid and liquid phases using a two-dimensional method: neither the sequence based on T_1-weighted FID-CPMG (Fig. 1c), nor the 2D reconstruction method, which needs the combination of various analytical functions, has ever been implemented. Moreover, applications of T_1–T_2 experiments have focused principally on samples with a small or no solid fraction.

We propose here an adaptation of the existing 2D reconstruction algorithm [29] in order to process T_1-weighted FID-CPMG datasets. We have therefore introduced a direct model based on a combination of the standard CPMG decreasing exponentials and Abragam's FID function in the reconstruction method [35–37]. We show that these developments lead to an accurate reconstruction of the IR-FID-CPMG relaxation time distributions using the Maximum Entropy Method in two dimensions (MEM2D) and provide more relevant information about the overall composition of complex samples as compared to the distribution obtained from CPMG data alone.

2. Experimental section

^{1}H NMR measurements were performed using a Time-Domain spectrometer (Minispec MQ20 Bruker, Germany) operating at a resonance frequency of 20 MHz and equipped with a 10 mm ^{1}H high-low variable temperature probe head (PH H20-10-33/RH1/GY3 with a dead-time of 11.6 μs, Bruker SA, Wissembourg, France). Magnetic field tuning, homogeneity of the magnet, detection angles, receiver gain and pulse lengths were checked for each sample. The NMR system was regulated using dried air, cooled in a dedicated cryostat (Julabo FP50-HP, Julabo Labortechnik GmbH, Germany) and heated by an electric resistance placed just at the bottom of the NMR tube and monitored by a dedicated temperature control device (BVT 3000, Bruker SA, Wissembourg, France). After having checked the good functioning of the spectrometer, the second daily experiment consisted in calibrating the temperatures of measuring in an oil tube. During the NMR experiments, the temperature was controlled each 30 s by placing an optic fiber directly into the sample (Neoptix Inc., Canada) allowing for ±0.1 K temperature precision. The thermal monitoring diagram for each sample ensured that there was no fluctuation in temperature during the NMR acquisition. Three kinds of sample were studied in duplicate: triacylglycerol and water (TAGW1 and TAGW2), starch–water model (SWM1, SWM2) and 45% hydrated wheat starch SW45 (both duplicates were discussed together). The experiments were performed, respectively, at 293 K and 279 K for SWM and TAGW samples, and at 293 and 363 K for SW45 samples. The 1D FID-CPMG and 2D IR-FID-CPMG signals were acquired, respectively, in phase-sensitive and single channel modes. The 90° pulse

was typically in the range of 2.5 μs and 16 scans were acquired with a recycle delay (RD) depending on the sample (see the figure legends). In order to avoid artefacts and to minimize B_1 inhomogeneity effects, small sample heights (app. 1 cm) were prepared and each sample was positioned in the homogeneous region of the radio-frequency coil. The inversion-recovery method was repeated for a range of τ_1 times to encode T_1 (typically 50 values) and CPMG pulse trains spaced by 0.2 or 0.6 ms echo time ($2.\tau_2$) depending on the sample. The FID was sampled for 152 μs and an acquisition sampling rate of 2.5 MHz.

Nickel sulfate hexahydrate ($NiSO_4{\cdot}6H_2O$ from VWR International S.A.S, Fontenay-sous-Bois, France) was used to prepare aqueous $NiSO_4$ solutions at concentrations of 1.3 and 17.6 mM, giving at 20 MHz and 293 K equal T_1 and T_2 of 1150 and 150 ms, respectively.

The TAGW model samples were prepared by introducing a 5 mm diameter NMR tube containing around 100 mg of doped water ($NiSO_4$ solution, expected $T_1 = T_2 = 1150$ ms) in a 10 mm NMR tube containing around 420 mg of anhydrous milk fat (gift from ENILIA, Surgères, France). The starch–water model sample (SWM) was prepared using a 10 mm diameter NMR tube containing around 225 mg of native wheat starch powder (purchased from Sigma–Aldrich, Saint-Quentin-Fallavier, France) and a 5 mm diameter NMR tube containing 122 mg of doped water ($NiSO_4$ solution, expected $T_1 = T_2 = 150$ ms). The water content of model samples were determined by NMR on the basis of the contribution of the characteristic water signal (in volts) to the total NMR signal and knowing the mass intensity of pure water measured in the same conditions, i.e. temperature and receiver gain (specified in the Result section) [38]. The 45% hydrated wheat starch sample (SW45) was prepared as in Rondeau-Mouro et al. [38]. The mixture was gently homogenized in a glass vial by stirring for 5 min using a small spatula. The dry matter and the water content of the SW sample were determined by measuring variations in their mass after drying in an oven at 103 °C for 24 h.

1D FID-CPMG relaxation curves were first analyzed by the Marquardt method based on least-squares nonlinear regression [39], implemented on Scilab (Scilab Enterprises, Versailles, France). The data were also fitted using the Maximum Entropy Method (MEM) both for 1D and 2D processing. This was performed on Matlab® (The MathWorks, Inc., Version R2006b 7.3.0.267) using the adequate algorithm (see the next section). All NMR measurements were expressed as spin–spin relaxation times (noted T_2, in ms) with their corresponding relative amplitudes or area under the peak (noted A, in percentages). Marginal distributions correspond to the computed T_1 and T_2 distributions of the joint distribution $S(T_1,T_2)$ according to $S(T_1) = \int S(T_1,T_2)dT_1$ and $S(T_2) = \int S(T_1,T_2)dT_2$.

3. Review of the algorithms

3.1. Reconstruction of T_1–T_2 distributions from IR-CPMG acquisition

Conventional T_1–T_2 NMR experiments are performed with a CPMG sequence after the inversion recovery (IR) block, as illustrated in Fig. 1b. In this pulse sequence, the recovery time τ_1 and the half-echo time τ_2 are independent time variables giving rise to the acquisition of the two-dimensional array $Y(\tau_1,\tau_2)$. The 2D NMR signal measured $Y(\tau_1,\tau_2)$ depends on the continuous distribution $S(T_1,T_2)$ of the T_1 and T_2 relaxation times according to the equation:

$$Y(\tau_1,\tau_2) = \iint k_1(\tau_1,T_1)S(T_1,T_2)k_2(\tau_2,T_2)\ dT_1\ dT_2 \tag{1}$$

where kernels k_1 and k_2 are related to the longitudinal and transverse relaxation times and their analytical expression depends on the NMR sequence used.

In the case of the classical IR sequence for T_1 and the CPMG sequence for T_2, the kernels are:

$$k_1(\tau_1,T_1) = 1 - \gamma.e^{-\tau_1/T_1} \tag{2}$$

$$k_2(\tau_2,T_2) = e^{-\tau_2/T_2} \tag{3}$$

where $\gamma = 1 - \cos\varphi$, with φ being the first flip angle (in radians) in the T_1 block. Using the IR sequence, γ is expected to be close to 2.

Eq. (1) can be seen as a 2D Laplace transform of the relaxation time distribution $S(T_1,T_2)$. In practice, only discrete values of τ_1 and τ_2 are considered and this equation is expressed using the matrix following the equation:

$$\boldsymbol{Y} = \boldsymbol{K}_1\boldsymbol{S}\,\boldsymbol{K}_2^t + \boldsymbol{E} \tag{4}$$

where matrix $\boldsymbol{E}$ corresponds to the measurement noise and model discretization errors, and matrix $\boldsymbol{S}$ contains a discretized version of the $S(T_1,T_2)$ distribution as expressed in Eq. (5):

$$[\boldsymbol{S}]_i^j = S(T_{1i},T_{2j}) \tag{5}$$

The elements of $\boldsymbol{K}_1$ and $\boldsymbol{K}_2$ are given by:

$$[\boldsymbol{K}_1]_i^j = k_1(\tau_{1i},T_{1j}) \quad \text{and} \quad [\boldsymbol{K}_2]_i^j = k_2(\tau_{2i},T_{2j}) \tag{6}$$

Estimation of the joint distribution $S(T_1,T_2)$ of the relaxation times requires the inversion of Eq. (4) in order to determine the matrix $\boldsymbol{S}$. However, such a problem corresponds to an ill-posed inverse problem, a numerical inversion of a Laplace transform [40]. The main reason is that matrices $\boldsymbol{K}_1$ and $\boldsymbol{K}_2$ are ill-conditioned. Consequently, a naive numerical inversion yields an unstable solution due to noise amplification and negative distribution amplitudes [41]. Solving the inverse problem using an NNLS algorithm is unfeasible since it requires the writing of the model in a linear form ($\boldsymbol{y} = \boldsymbol{K}\,\boldsymbol{s} + \boldsymbol{e}$), with a huge matrix $\boldsymbol{K} = \boldsymbol{K}_1 \otimes \boldsymbol{K}_2$. The

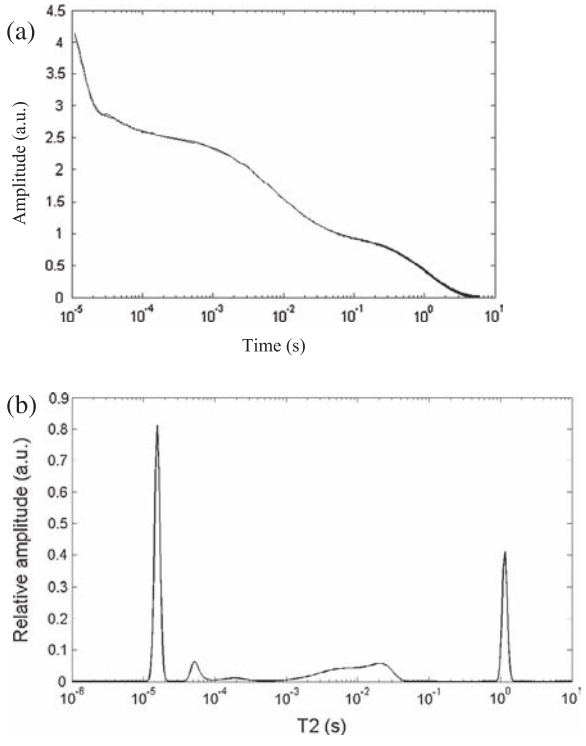

Fig. 2. NMR signal (solid line) and curve fitting (dashed line) on logarithmic time axis of 1D FID-CPMG (a) and corresponding T_2 distribution by signal fitting based on Eq. (11) (b) of triacylglycerol–water sample (TAGW2). Temperature = 279 K. The FID was sampled for 152 μs at a sampling rate of 0.4 μs per point. 10,000 echoes were recorded with an echo time of 0.6 ms, RD = 6 s. Number of iterations 277, khi^2 0.016312, RMSE 0.015112, $\omega = 2.25$ rad.

Table 1
T_2 (ms) and A (%) values from the MEM fitting of 1D FID-CPMG data of TAGW and SWM samples. Values in italic are standard errors calculated on the basis of two samples (TAGW1, TAGW2 and SWM1, SWM2).

Sample	T_2 (1)	A (1)	T_2 (2)	A (2)	T_2 (3)	A (3)	T_2 (4)	A (4)	T_2 (5)	A (5)
TAGW	**1.61E−02**	**38.92%**	**4.93E−02**	**5.78%**	**1.73E−01**	**3.33%**	**1.93E+01**	**31.99%**	**1.16E+03**	**19.96%**
	5.15E−04	*3.47%*	*4.69E−03*	*0.21%*	*2.09E−02*	*1.07%*	*2.80E+00*	*1.92%*	*7.07E+00*	*0.28%*
SWM	**2.42E−02**	**36.66%**	**7.20E−02**	**1.52%**	**5.53E−01**	**11.66%**	**1.50E+02**	**49.69%**		
	5.66E−06	*0.85%*	*3.58E−04*	*0.24%*	*1.49E−02*	*0.34%*	*4.95E−02*	*1.47%*		

Table 2
Water content (%) of TAGW and SWM determined from the MEM fitting of 1D FID-CPMG data (Eq. (11)) and 2D reconstruction of IR-FID-CPMG data (from the T_1 distribution (Eq. (2)) or the T_2 distribution (Eq. (12))). The water mass intensity was, respectively, 11.25 V/g and 10.66 V/g for TAGW (279 K) and SWM (293 K) samples for a receiver gain of 70DB. Values in italic are standard errors calculated on the basis of two samples (TAGW1, TAGW2 and SWM1, SWM2).

	TAGW_1D_T2	TAGW_2D_T1	TAGW_2D_T2	SWM_1D_T2	SWM_2D_T1	SWM_2D_T2
NMR	**20.75%**	**20.23%**	**20.23%**	**36.39%**	**37.30%**	**36.81%**
	0.12%	*0.36%*	*0.36%*	*1.63%*	*1.74%*	*1.74%*
Gravimetry		**19.42%**			**35.28%**	
		0.08%			*1.56%*	

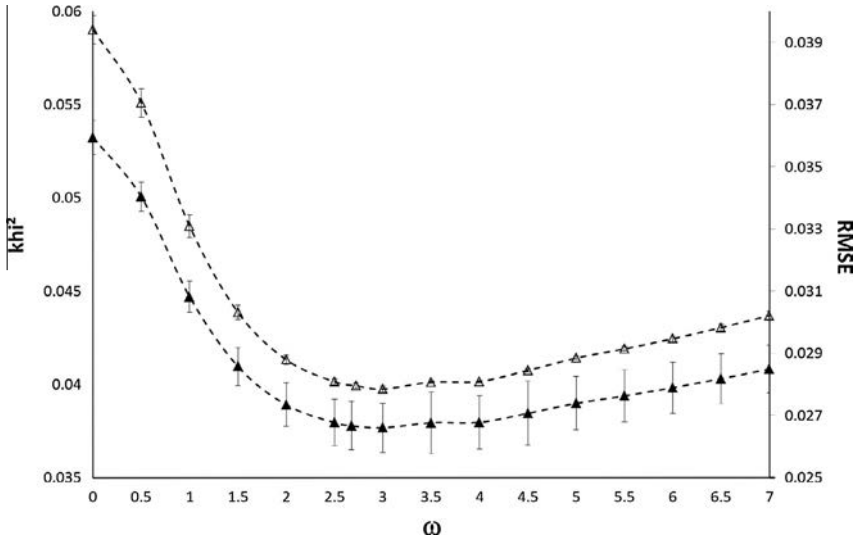

Fig. 3. Variation in khi^2 criterion (black triangle) and RMSE (open triangle) resulting from the MEM fitting of 1D FID-CPMG data from SWM. Fitting based on Eq. (11). Number of iterations 283 ± 3 to 228 ± 1.

approach proposed in [29] adds a Tikhonov regularization, but its implementation requires a data compression step to reduce the matrix dimension, which in practice may lead to the loss of information. An alternative approach to avoid data compression is to regularize the inverse problem by formulating the solution as the minimizer of a penalized least squares criterion, as shown in Eq. (7):

$$J(S) = \|\boldsymbol{Y} - \boldsymbol{K}_1\boldsymbol{S}\,\boldsymbol{K}_2^t\|_F^2 + \lambda R(S) \tag{7}$$

where $R(S)$ is the regularization term allowing encoding of some desirable properties of the solution [32]. In order to encode positivity, sparsity and smoothness of the joint distribution, we used a regularization function based on the maximum entropy principle [42–44], i.e.

$$R(S) = \sum_i \sum_j S_{ij} \log S_{ij} \tag{8}$$

To solve the large-scale optimization problem, an efficient method based on a truncated Newton algorithm was proposed in [29]. The main feature of this iterative method is to manage the memory storage and computation complexity in such a way as to solve the problem directly without data matrix factorization or compression. Moreover, an automatic tuning strategy for the regularization parameter λ was adopted (see Section IV.A.5 of [29] for more details). This strategy is based on the khi^2_{index} defined as:

$$khi^2_{index}(S) = \frac{\|\boldsymbol{K}_1\boldsymbol{S}\,\boldsymbol{K}_2^t - \boldsymbol{Y}\|_F^2}{\sigma^2} \tag{9}$$

where σ^2 is an estimate of the noise variance and S the reconstructed distribution for a fixed value of λ. The regularization parameter is chosen in such a way as to obtain a solution S leading to a khi^2_{index} equal to a predefined khi^2_{aim}. However, since the estimation of the noise variance can be inaccurate, an additional stopping criterion is to detect when the variation of λ leads to a small variation in the khi^2_{index}. Finally, the accuracy of the data fitting is assessed by computing the relative mean square error (RMSE) defined by:

$$\mathrm{RMSE}(S) = \frac{\|\boldsymbol{K}_1\boldsymbol{S}\,\boldsymbol{K}_2^t - \boldsymbol{Y}\|_F^2}{\|\boldsymbol{Y}\|_F^2} \tag{10}$$

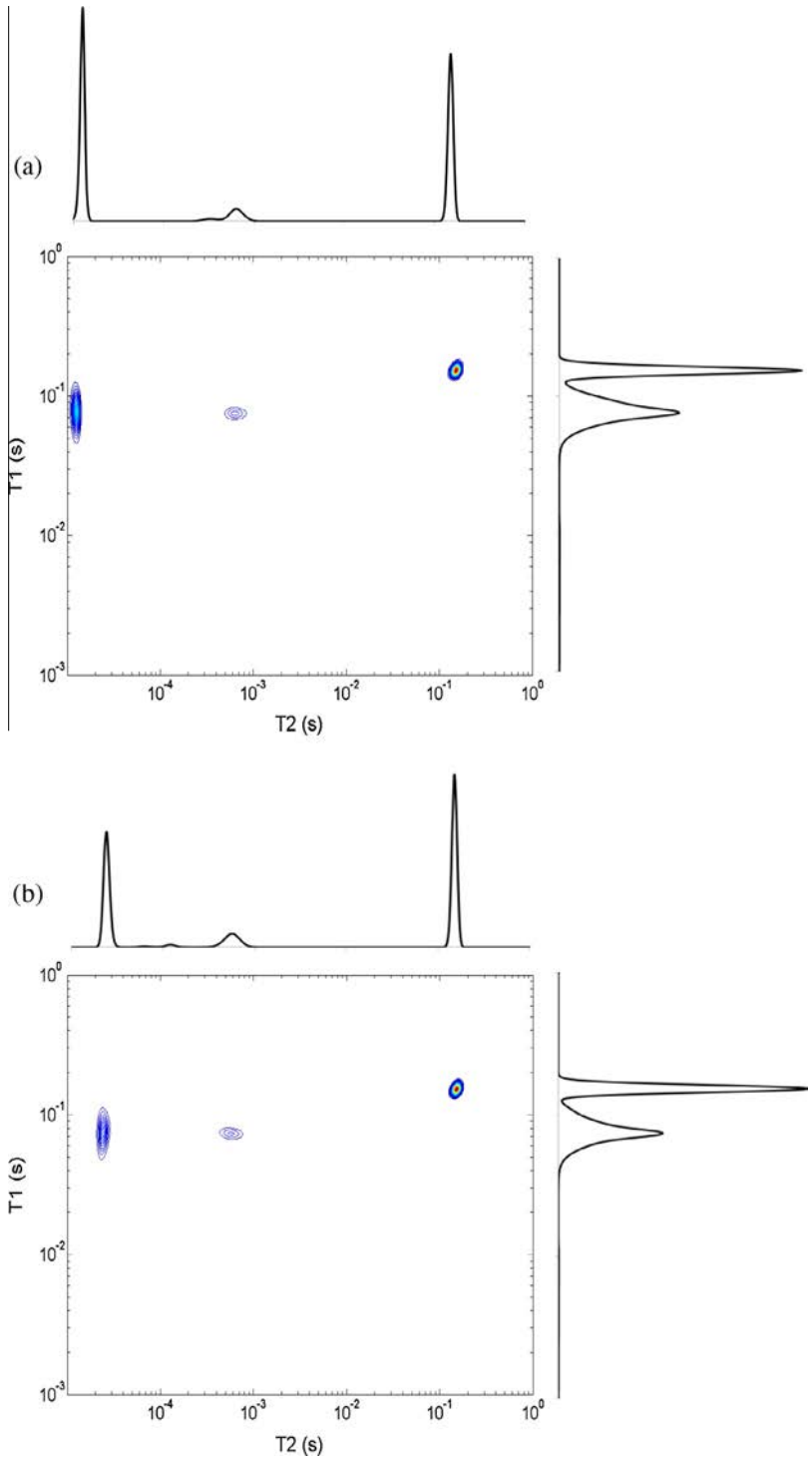

Fig. 4. 2D IR-FID-CPMG of SWM2 for ω = 0 rad (a) and ω = 2.72 rad (b). Temperature 293 K. 2D NMR experiments were performed using 50 values of τ_1 times between 5 ms and 1000 ms, 6000 echoes using an echo time $2.\tau_2$ of 0.2 ms, RD = 1 s. Reconstruction based on Eqs. (2) and (12) using φ = 180° in Eq. (2). Number of iterations 1000 for ω = 0 and ω = 2.72; khi^2 4.0115 for ω = 0 and 3.4508 for ω = 2.72; RMSE 0.1107 for ω = 0 and 0.0952 for ω = 2.72.

3.2. Reconstruction of T_1–T_2 distributions from IR-FID-CPMG acquisition

In the case of the acquisition of the FID signal, we propose the following k_2 kernel:

$$k_2(\tau_2, T_2) = \left(e^{\frac{-\tau_2}{T_2}} + e^{\frac{-\tau_2^2}{T_2^2}} \right) \cdot sinc\left(\frac{\omega}{T_2} . \tau_2 \right) \tag{11}$$

where *sinc* is the cardinal sine function ($sin\,(x)/x$) and ω the function angle equal to or greater than 0.

According to this model, the FID signal is described by the combination of a Gaussian broadening ($T_{2\text{Gauss}}$) and an exponential decay ($T_{2\text{exp}}$), both modulated by a Pake function [36]. The originality of this new algorithm is that it takes into account a *sinc* modulation of exponential decays throughout the FID signal. In Eq. (11), the short T_2 and the frequency of the *sinc* function are parameters that depend on each other. The frequency of the *sinc* function

Table 3
Area (A in %), T_1 (ms) and T_2 (ms) values determined on the marginal spectra obtained by 2D reconstruction (Figs. 4 and 5) of IR-FID-CPMG data from SWM at 293 K and SW45 samples at 293 K and 363 K. Values in italic are standard errors calculated on the basis of two samples.

Component no.	1	2	3	4	
SWM 293 K					
T_2	**0.024**	**0.073**	**0.536**	**150.4**	
	0.001	*0.008*	*0.000*	*0.0*	
$A(T_2)$	**36.69%**	**1.70%**	**11.47%**	**50.14%**	
	1.47%	*0.49%*	*0.30%*	*1.65%*	
		1		2	
T_1		**74.7**		**152.7**	
		4.0		*0.0*	
$A(T_1)$		**50.44%**		**49.56%**	
		1.61%		*1.61%*	
	1	2	3	4	
SW45 293 K					
T_2	**0.018**	**0.098**	**1.97**	**13.9**	
	0.001	*0.010*	*0.10*	*2.0*	
$A(T_2)$	**30.30%**	**4.05%**	**19.25%**	**46.40%**	
	0.30%	*2.00%*	*1.00%*	*3.00%*	
			1		
T_1			**165.0**		
			0.0		
$A(T_1)$			**100.0**		
			0.0		
	1	2	3	4	5
SW45 363 K					
T_2	**0.017**	**0.113**	**1.42**	**12.9**	**45.9**
	0.001	*0.010*	*0.40*	*1.0*	*3.0*
$A(T_2)$	**5.69%**	**5.29%**	**12.81%**	**74.17%**	**2.05%**
	1.00%	*0.50%*	*3.00%*	*2.00%*	*0.20%*
			1		
T_1			**228.0**		
			7.0		
$A(T_1)$			**88.90%**		
			1.00%		
			2		
	T_1		**42.2**		
			10.0		
	$A(T_1)$		**11.10%**		
			1.00%		

depends on both the number of dipolar interactions and the distance between dipoles, so it is clearly related to the short T_2 that characterizes non-random molecular motions, the latter being modulated by molecular structures and assemblies [35,45]. Actually, the proposed k_2 kernel (Eq. (11)) cannot be separated into two different kernels for shorter and longer T_2 in the FID signal (T_{2Gauss} and T_{2exp} variables, respectively). In effect, we assume that for very short T_2 values (T_{2Gauss}), the contribution of the exponential term should be almost constant and for longer T_2 values related to T_{2exp}, the Gaussian component should be almost equal to zero. In Eq. (11), the ω value can be adjusted in order to obtain the best fitting of the 2D data. However, this tuning step can be time-consuming (depending on the computer processor) and can be avoided for the analysis of some samples. For instance, in hydrated samples, ω is fixed at 0, since only the Gaussian function with decreasing exponential is necessary to adjust the FID signal. On the other hand, for solid samples, the ω parameter can be determined from the NNLS fitting of 1D FID data (see below for an example).

For the processing of FID-CPMG data, the continuity between the FID and CPMG signals is ensured by the concatenation of both (3) and (11) kernel equations which provides the kernel:

$$k_2(\tau_2, T_2) = \begin{cases} \alpha\left(e^{\frac{-\tau_2}{T_2}} + e^{\frac{-{\tau_2}^2}{{T_2}^2}}\right).sinc\left(\frac{\omega}{T_2}.\tau_2\right) & if\ \ \tau_2 \le \tau_{fid} \\ (1-\alpha)e^{\frac{-\tau_2}{T_2}} & if\ \ \tau_2 > \tau_{fid} \end{cases} \quad (12)$$

where α is the continuity parameter at τ_{fid}, which is the upper time limit of the FID signal (last point of FID). Finally, the reconstruction of IR-FID-CPMG maps is performed using kernels from Eqs. (2) and (12).

4. Results and discussion

The new sequence IR-FID-CPMG illustrated in Fig. 1c and the algorithm based on Eqs. (2) and (12) were tested on model samples constituted of classical food ingredients, i.e., water, fats, and starch. The aim was to mimic physically compartmentalization of water or to create a multiphasic system where water and others constituents were not influenced by each other, or in other terms, did not interact. Two model samples were therefore prepared based on the physical separation of these ingredients, i.e., water vs fats and water vs starch, and a third sample comprised a mixture of water and starch, thus representing the basic mixture of a classical dough system for bread making (hydrated at 45 wt% of water). The first validation step of the fitting method consisted of fitting of the 1D FID-CPMG data acquired using the classical FID-CPMG sequence illustrated in Fig. 1a and the newly developed maximum entropy method using the reconstruction algorithm based on Eq. (11). The FID-CPMG sequence couples the FID acquisition classically performed for the determination of solid content in fats and oils [9] and a CPMG pulse train allowing T_2 relaxation time measurements for mobile protons (liquid phase) independently of field inhomogeneities. To achieve the detection of fast-decaying components (such as solids) in FID, the TD-NMR spectrometers are now equipped with (i) a high-power transmitter generating very short 90° pulses, (ii) a short dead time of few microseconds (less than 20 μs), and (iii) fast digitalization (20 MHz) allowing the acquisition of a sufficient number of data points in the steepest part of the FID. Moreover, because the TD-spectrometers operate at low fields (<1 T), it has become possible to measure short T_2 relaxation times less influenced by susceptibility differences.

In effect, as already shown by Trezza et al., the TD-NMR inhomogeneity can easily be determined on a liquid sample and has been shown to be characterized by a Gaussian decay with a T_2^* of 0.5–2 ms, which corresponds to a FID factor correction of less than 5% [17].

Fig. 2a presents the time evolution of the FID-CPMG signal represented on a logarithmic time axis for one triacylglycerol–water sample (TAGW2) at 279 K. As in the case of inorganic crystals, glasses and solid-state polysaccharides (see references in [35,45]), a small beat pattern or oscillation was observed for short times. This specific signal pattern arises from residual local orders between near neighbor triacylglycerol (TAG) protons. This short-range organization induces strong dipolar interactions between protons that are characterized by the second dipolar moment M_2. This parameter provides information about TAG motion involved in intra- and intermolecular dipolar interactions between chains and the nanostructure of TAG crystals [26]. Indeed, as pointed out by Abragam [36], the NMR spectrum of the TAG protons is well represented by the combination of a *sinc* function and Gaussian broadening following Eq. (11), where ω is the *sinc* function angle and T_2 the spin–spin relaxation time of TAG protons. Estimation of ω could be performed by using the $T_2(1)$ and the *sinc* frequency value adjusted with the NNLS method.

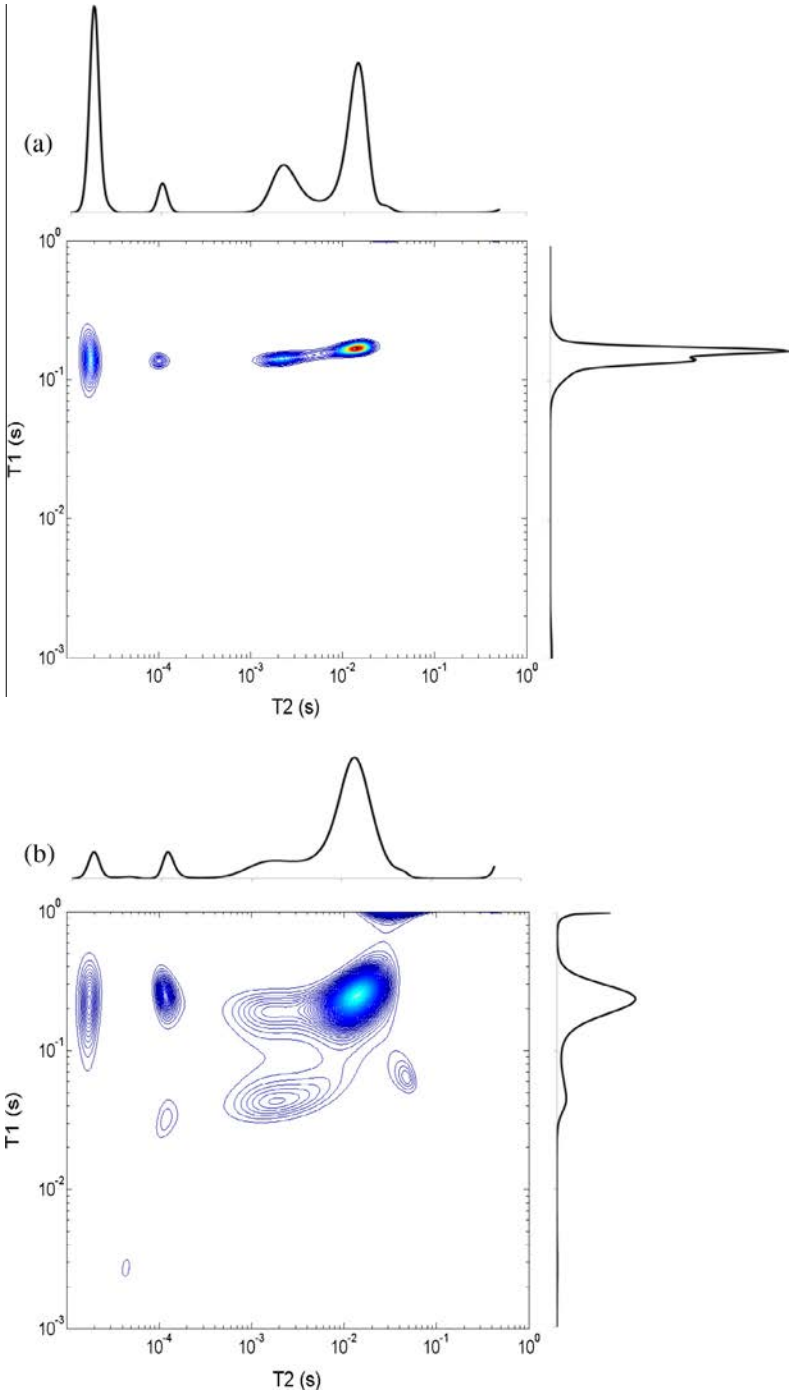

Fig. 5. 2D IR-FID-CPMG of SW45 at 293 K (a) and 363 K (b). 2D NMR experiments were performed using 50 values of τ_1 times between 5 ms and 1500 ms, 800 echoes using echo time $2.\tau_2$ of 0.2 ms, RD = 1.5 s. Reconstruction based on Eqs. (2) and (12) using $\varphi = 172°$ in Eq. (2). Number of iterations 1000; $\omega = 0$ rad; khi^2 0.3267 at 293 K and 0.3769 at 323 K; RMSE 0.0114 at 293 K and 0.0083 at 323 K.

In the case of TAGW samples, ω was 2.37 ± 0.16 rad. The rest of the signal for longer times, acquired with a CPMG train, can easily be fitted by decreasing exponentials. The result of this fitting is presented in Fig. 2b, showing the T_2 distribution with four well-resolved peaks at short and long relaxation times, while a wide distribution was obtained between 1 and 100 ms. The NNLS fitting resulted in five discrete values of T_2 (Table 1). Four of them (between 10^{-2} and 10^{2} ms) were characteristic of TAG protons [17,26], and the longest T_2 relaxation time at 1163 ± 7.1 ms, with a peak area of 19.96 ± 0.28%, corresponded to doped water. The T_2 of doped water was 1163 ms, which is very close to the expected value (1150 ms).

The MEM fitting of T_2 components for TAGW at 279 K was remarkably good, demonstrated not only through the peak position in agreement with the NNLS fitting, in particular for doped water, but also by measuring the relative area under each peak. Indeed, the water content in the sample could be estimated on the basis of the area of the corresponding T_2 peak and knowing the mass intensity of pure water in the same conditions (11.25 V/g, for a receiver gain of 70 dB at 279 K for example). Based

on the T_2 measurements, the water content was 20.75 ± 0.12%, compared to 19.42 ± 0.08% using gravimetry (Table 2).

The FID-CPMG signal was also acquired and processed for two starch–water model samples (SWM1 and SWM2) at 293 K. In order to validate the MEM fitting, a step-by-step change of the ω value was performed. Fig. 3 shows variations in the criterion values khi^2 and RMSE as a function of the FID value ω in Eq. (11) when processing the FID-CPMG signal of SWM1 and SWM2. The two criteria decreased to an optimum value around 2.5–3 rad, before increasing for higher ω values to 7 rad. The average values resulting from the MEM fitting of 1D FID-CPMG data measured on SWM samples are shown in Table 1. The standard deviations indicate very close T_2 and A values, thus demonstrating the good repeatability of the sample preparation and also the repeatability of measurements and the fitting method used.

Fig. 4 shows 2D IR-FID-CPMG maps and corresponding marginal T_1 and T_2 distributions after processing and reconstruction using Eqs. (2) and (12) for the SWM2 sample. Compared to the classical 2D IR-CPMG experiment illustrated in Fig. 1b, the new IR-FID-CPMG sequence (Fig. 1c) lasted nearly the same time (7.6 ms extra). It consists in the acquisition of T_1-weighted FID-CPMG signals using the inversion recovery sequence as a first pulse block ($180°$-τ_1-) followed by a FID acquisition ($90°$-τ_{FID}-) before the CPMG train (τ_2-[180-τ_2]$_n$) where n is the echo number. Therefore, this sequence needs, as for the 1D FID-CPMG sequence (Fig. 1a), the opening of the receiver gate just before the echoes train and for each echo. Fig. 4a and b corresponds to the processing performed for two different ω values in Eq. (12), when the ω values were 0 and 2.72 rad, respectively. The latter corresponds to the ω value calculated from the NNLS fitting of 1D data, which is the recommended method to determine ω. The marginal T_2 distributions revealed an inversion of amplitude between the short and the long T_2 peaks. Clearly, the value of ω greatly affects the results and should be determined for each sample. Study of the peak position (Table 3) as well as calculation of the water content based on marginal T_2 and T_1 spectra (Table 2) confirmed that the ω value of 2.70 ± 0.03 rad gave a good 2D reconstruction.

Indeed, the water content, calculated using the T_2 and T_1 peak area from 2D data of SWM samples, was, respectively, 37.30 ± 1.74% and 36.81 ± 1.74% compared to the 35.28 ± 1.56% measured moisture by sample drying and gravimetry. The 2D reconstruction of the data recorded on TAGW samples (not shown), confirmed the robustness of the new processing since the calculated water content based on the peak area of T_2 and T_1 distributions corresponded to the expected values of 19.42 ± 0.08% (Table 2).

In order to validate this new 2D reconstruction model on a real product close to dough in bread making, we also tested the 2D reconstruction following Eqs. (2) and (12) on a 45% hydrated starch sample (SW) at ambient temperature and also upon heating. Fig. 5a and b shows the reconstructed 2D map as well as the marginal T_1 and T_2 distributions obtained from the reconstruction of IR-FID-CPMG data acquired on SW45 at 293 K and 363 K, respectively. At 293 K, one T_1 value was found at 165 ms (Fig. 5a). The T_2 values corresponded to the expected relaxation times estimated by Rondeau et al. using the 1D FID-CPMG sequence [38]. While $T_2(1)$ and $T_2(2)$ were assigned to starch protons and highly organized water molecules (“channel water” in crystalline phases [46]), the added water phase was characterized by $T_2(3)$ and $T_2(4)$ at 293 K. Calculation of the water content at this temperature on the basis of the peak area for $T_2(3)$ and $T_2(4)$ (measured in marginal spectra) resulted in 48.43 ± 0.54% hydration that was slightly overestimated compared to the expected 45 wt% in the SW45 sample. This result demonstrates the difficulty of measuring quantitative data from highly hydrated samples that may suffer some sedimentation while acquiring the 2D data. In effect, intact starch granules are not soluble in cold water. For water content higher than 45 wt% and for long acquisition times (>1 H), granules can sediment on the bottom of the NMR tube. In addition, higher the water content is, longer the recycle delay should be because of a large amount of extra-granular water (in opposite to intra-granular water for water inside starch granules). At 363 K, a fifth T_2 value was observed at 45.9 ms, representing 2.05% of the total signal (Fig. 5b). The T_1 value increased with temperature but a shorter T_1 at 42.2 ms was also observed and assigned to cross-relaxation mechanisms [47]. While the longer T_1 value was correlated at $T_2(1)$ to $T_2(4)$, as observed at 293 K, the shorter T_1 time at 42.2 ms showed cross-peaks with the T_2 relaxation time characteristics of water and gelatinized starch protons, highlighting numerous chemical exchanges and dipolar interactions between water and starch, especially when the latter was gelatinized.

5. Conclusions

We have presented here an adaptation of an efficient inversion method based on maximum entropy regularization in order to reconstruct 2D T_1–T_2 correlation maps obtained using the new IR-FID-CPMG sequence. We demonstrated that the insertion of an adapted Abragam’s FID function into the 2D Laplace inversion algorithm was remarkably effective for quantitative analysis of IR-FID-CPMG data. In this processing step, the sine function angle value (ω) can be adjusted or determined from the NNLS fitting of 1D FID data, this latter option being faster (few minutes compared to one hour for five well-chosen ω values). The acquisition of IR-FID-CPMG data was as long as that using the classical IR-CPMG sequence, but it was shown to assist the characterization of complex samples composed of solid and liquid phases such as fats and starchy products. As long as samples contain a moderate liquid content, this method can be applied to monitor structural changes during a particular process, such as heating. The implementation of FID acquisitions in 2D not only resolves short T_2 relaxation times related to strong dipolar interactions in solid phases, but also considers the NMR signal of each component whatever its physical state, making possible the quantification of molecules using the area of the relaxation time peak. Another advantage of the IR-FID-CPMG method concerns its ability to distinguish between solid phases having different T_1 relaxation times. It permits also to demonstrate some cross-relaxation phenomena. This is the case of many samples containing highly hydrophilic molecules like proteins or polysaccharides that display, with water, chemical exchanges and dipolar interactions. We believe that this new sequence and the processing proposed will assist the scientific community in studying multiphasic or compartmentalized samples both in food science and in biology and material sciences.

Acknowledgments

This work was performed using the NMR facilities of the PRISM Research Platform (Rennes, France). The authors thank the Regional Council of Brittany of France for their financial support.

References

[1] IUPAC, Norm Version 2.150 (ex 2.323): solid content determination in fats by NMR (low resolution nuclear magnetic resonance), 1987.
[2] ISO, 8292: 1991(E) International standard: animal and vegetable fats and oils – determination of solid fat content – pulsed nuclear magnetic resonance method/first edition 1991-12-01, 1991.
[3] AOCS, Official Method Cd 16b-93: Solid Fat Content (SFC) by Low Resolution Magnetic Resonance.
[4] H.Y. Carr, E.M. Purcell, Effects of diffusion on free precession in nuclear magnetic-resonance experiments, Curr. Cont./Phys. Chem. Earth Sci. (1954). 24-24.

[5] S. Meiboom, D. Gill, Modified spin-echo method for measuring nuclear-relaxation times, Curr. Cont./Eng. Technol. Appl. Sci. (1958). 16-16.
[6] R.L. Vold, J.S. Waugh, M.P. Klein, D.E. Phelps, Measurement of spin relaxation in complex systems, J. Chem. Phys. 48 (1968) 3831–3832.
[7] C. Rondeau-Mouro, A. Delahaye, M. Cambert, L. Fournaison, F. Mariette, Characterization of solid content and distinction between type A and B crystals of TBAB hydrates by time domain NMR, Chem. Eng. Sci. 138 (2015) 544–551.
[8] J. Mitchell, L.F. Gladden, T.C. Chandrasekera, E.J. Fordham, Low-field permanent magnets for industrial process and quality control, Prog. Nucl. Magn. Reson. Spectrosc. 76 (2014) 1–60.
[9] M.C.M. Gribnau, Determination of solid/liquid ratios of fats and oils by low-resolution pulsed NMR, Trends Food Sci. Technol. 3 (1992) 186–190.
[10] W.P. Halperin, Pore structure of hydrating cement paste by magnetic resonance relaxation analysis, Abs. Pap. Am. Chem. Soc. 210 (1995) 59-IEC.
[11] L.L. Latour, R.L. Kleinberg, P.P. Mitra, C.H. Sotak, Pore-size distributions and tortuosity in heterogeneous porous media, J. Magn. Reson. 112 (1995) 83–91.
[12] P.P. Mitra, P.N. Sen, Effects of microgeometry and surface relaxation on NMR pulsed-field-gradient experiments: simple pore geometries, Phys. Rev. B 45 (1992) 143–156.
[13] I. Saha, J. Franck, T. Hopper, B. Sun, Y.-Q. Song, Uncertainties in the measurement of rock porosity obtained from Laplace inversion of NMR relaxation logs, Petrophysics 50 (2009) 345–351.
[14] Y.Q. Song, H. Cho, T. Hopper, A.E. Pomerantz, P.Z. Sun, Magnetic resonance in porous media: recent progress, J. Chem. Phys. 128 (2008).
[15] K.E. Washburn, C.H. Arns, P.T. Callaghan, Pore characterization through propagator-resolved transverse relaxation exchange, Phys. Rev. E 77 (2008).
[16] B.P. Hills, K.M. Wright, P.S. Belton, Proton NMR-studies of chemical and diffusive exchange in carbohydrate systems, Mol. Phys. 67 (1989) 1309–1326.
[17] E. Trezza, A.M. Haiduc, G.J.W. Goudappel, J.P.M. van Duynhoven, Rapid phase-compositional assessment of lipid-based food products by time domain NMR, Magn. Reson. Chem. 44 (2006) 1023–1030.
[18] F. Mariette, Investigations of food colloids by NMR and MRI, Curr. Opin. Coll. Interf. Sci. 14 (2009) 203–211.
[19] F. Mariette, T. Lucas, NMR signal analysis to attribute the components to the solid/liquid phases present in mixes and ice creams, J. Agricult. Food Chem. 53 (2005) 1317–1327.
[20] C.L. Lawson, R.J. Hanson, Solving Least Squares Problems, Prentice Hall, Englewood Cliffs, NJ, 1974.
[21] S.W. Provencher, CONTIN: a general purpose constrained regularization program for inverting noisy linear algebraic and integral equations, Comput. Phys. Commun. 27 (1982) 229–242.
[22] R.L. Parker, Y.Q. Song, Assigning uncertainties in the inversion of NMR relaxation data, J. Magn. Reson. 174 (2005) 314–324.
[23] M. Prange, Y.-Q. Song, Quantifying uncertainty in NMR T-2 spectra using Monte Carlo inversion, J. Magn. Reson. 196 (2009) 54–60.
[24] M. Prange, Y.-Q. Song, Understanding NMR T-2 spectral uncertainty, J. Magn. Reson. 204 (2010) 118–123.
[25] Y.-Q. Song, Resolution and uncertainty of Laplace inversion spectrum, Magn. Reson. Imag. 25 (2007) 445–448.
[26] J. van Duynhoven, I. Dubourg, G.J. Goudappel, E. Roijers, Determination of MG and TG phase composition by time-domain NMR, J. Am. Oil Chem. Soc. 79 (2002) 383–388.
[27] D. Bernin, D. Topgaard, NMR diffusion and relaxation correlation methods: new insights in heterogeneous materials, Curr. Opin. Coll. Interf. Sci. 18 (2013) 166–172.
[28] A.E. English, K.P. Whitthall, M.L.G. Joy, R.M. Henkelman, Quantitative two-dimensional time correlation relaxometry, Magn. Reson. Med. 22 (1991) 425–434.
[29] E. Chouzenoux, S. Moussaoui, J. Idier, F. Mariette, Efficient maximum entropy reconstruction of nuclear magnetic resonance T1–T2 spectra, IEEE Trans. Signal Process. 58 (2010) 6040–6051.
[30] P.J. Hore, NMR data processing using the maximum entropy method, J. Magn. Reson. 62 (1985) 561–567.
[31] S. Sibisi, Two-dimensional reconstructions from one-dimensional data by maximum entropy, Nature 301 (1983) 134–136.
[32] L. Venkataramanan, Y.Q. Song, M.D. Hurlimann, Solving Fredholm integrals of the first kind with tensor product structure in 2 and 2.5 dimensions, IEEE Trans. Signal Process. 50 (2002) 1017–1026.
[33] H. Peemoeller, M.M. Pintar, Nuclear magnetic resonance multiwindow analysis of proton local fields and magnetization distribution in natural and deuterated mouse muscle, J. Magn. Reson. 28 (1979) 339–356.
[34] H. Peemoeller, M.M. Pintar, Two-dimensional time-evolution approach for resolving a composite free-induction decay, J. Magn. Reson. 41 (1980) 358–360.
[35] W. Derbyshire, M. van den Bosch, D. van Dusschoten, W. MacNaughtan, I.A. Farhat, M.A. Hemminga, J.R. Mitchell, Fitting of the beat pattern observed in NMR free-induction decay signals of concentrated carbohydrate-water solutions, J. Magn. Reson. 168 (2004) 278–283.
[36] A. Abragam, The Principle of Nuclear Magnetism, Clarendon Press, Oxford, 1961.
[37] G.W. Parker, F. Lado, Calculation of NMR line shapes in calcium fluoride from modified moments expansions, Phys. Rev. B 9 (1974) 22–28.
[38] C. Rondeau-Mouro, M. Cambert, R. Kovrlija, M. Musse, T. Lucas, F. Mariette, Temperature-associated proton dynamics in wheat starch-based model systems and wheat flour dough evaluated by NMR, Food Bioproc. Technol. 8 (2015) 777–790.
[39] D.W. Marquardt, An algorithm for least-squares estimation of nonlinear parameters, J. Soc. Indust. Appl. Math. 11 (1963) 431–441.
[40] Y. Song, Laplace inversion for NMR data analysis, Magn. Reson. Food Sci.: Food Thought (2013) 25–31.
[41] R. Lamanna, On the inversion of multicomponent NMR relaxation and diffusion decays in heterogeneous systems, Conc. Magn. Reson. Part A 26 (2005) 78–90.
[42] U. Amato, W. Hughes, Maximum-entropy regularization of Fedholm integral-equations of the 1st kind, Inv. Prob. 7 (1991) 793–808.
[43] F. Mariette, J.P. Guillement, C. Tellier, P. Marchal, Continuous relaxation time distribution decomposition by MEM, in: R.D. N., Ed. (Ed.) Signal Treatment and Signal Analysis in NMR, Elsevier, Paris, 1996, pp. 218–234.
[44] J. Skilling, R.K. Bryan, Maximum-entropy image-reconstruction: general algorithm, Mon. Not. R. Astron. Soc. 211 (1984) 111–124.
[45] R.F. Ying, L. Saulnier, C. Rondeau-Mouro, Films of arabinoxylans and β-glucans extracted from cereal grains: molecular motions by TD-NMR, Carbohyd. Polym. 86 (2011) 812–822.
[46] H.R. Tang, J. Godward, B. Hills, The distribution of water in native starch granules – a multinuclear NMR study, Carbohyd. Polym. 43 (2000) 375–387.
[47] S.F. Tanner, B.P. Hills, R. Parker, Interactions of sorbed water with starch studied using proton nuclear magnetic resonance spectroscopy, J. Chem. Soc., Faraday Trans. 87 (1991) 2613–2621.